SAND2017-13531C

Uncertainty Quantification of Wind Turbine Blade Load Measurement, Estimation, and Transformation

Brandon L. Ennis*, Joshua A. Paquette†, and Jonathan R. White†

Sandia National Laboratories‡, Albuquerque, NM, 87185, USA

This paper describes the process of transforming measured blade loads, with force estimation, to wind turbine quantities of interest. Uncertainty quantification on the blade load measurement and force estimation is derived and used to estimate uncertainty on aerodynamic torque and rotor thrust for sample cases. A methodology is defined for calculating mean values and quantifying the uncertainty in these important quantities of interest for wind turbines when your available data includes only blade root moment measurements. This paper is not intended to provide precise values for these uncertainties at the current stage, however, sample measurement uncertainties are defined and used along with representative mean values to identify the sensitivity of uncertainty in torque and thrust to the constituent variables and associated uncertainties. The largest contributors of the uncertainty when using blade strain gage measurements to estimate rotor loads is identified for the sample cases revealing the components that have the largest effect on the resulting quantity of interest's uncertainty, and those which have negligible effect on the uncertainty.

Nomenclature

DOE	Department of Energy
SNL	Sandia National Laboratories
$SWiFT$	Scaled Wind Farm Technology
ϵ	Axial strain
γ	Shear strain
θ	Strain gage misalignment angle
ν	Poisson's ratio
E	Young's modulus
I	Area moment of inertia
CTE	Coefficient of thermal expansion
G	Shear modulus
J	Polar moment of inertia
F_G	Strain gage factor
λ_0	Fiber optic sensor nominal wavelength
K_{cal}	Calibration constant from differential strain to bending moment
C_l	Coefficient of lift
C_d	Coefficient of drag
c	Chord length
a	Axial induction factor
a'	Tangential induction factor
l	Blade length
τ	Torque

*Senior Member of the Technical Staff, Wind Energy Technologies, PO Box 5800, MS 1124, Member AIAA.

†Principal Member of the Technical Staff, Wind Energy Technologies, PO Box 5800, MS 1124, Member AIAA.

‡Sandia National Laboratories is a multimission laboratory managed and operated by National Technology and Engineering Solutions of Sandia, LLC., a wholly owned subsidiary of Honeywell International, Inc., for the U.S. Department of Energy's National Nuclear Security Administration under contract DE-NA-0003525.

T	Thrust
$\theta_{rotorplane}$	Angle between strain gage pair and blade rotational plane, at zero pitch
β_0	Blade pitch angle
$\theta_{precone}$	Blade precone angle
d_{gage}	Distance from strain gage location to rotor hub axis
ψ	Blade azimuth angle
$\theta_{shafttilt}$	Wind turbine shaft tilt angle
m_B	Blade mass
r_{CG}	Blade center of gravity, in rotor coordinates
Ω	Rotor rotational speed
Subscript	
s	Measured sensor value
B	Value for a single blade
rotor	Value for the entire rotor
X, Y, Z	Global coordinate system in rotor rotational plane
x', y', z'	Local coordinate system representing strain gage mounting location

I. Introduction

Individual wind turbine blade loads produce valuable information on a turbine's load state. This information is gradually reduced as you move the load measurement to other locations, such as a rigid drive shaft that combines the individual blade loads together and structurally dampens the high frequency response content. At other measurement locations what is measured is actually different from what was intended. For example, comparing aerodynamic power with electrical power after bearing, gearbox, and generator losses. In addition to the higher resolution data content, the value of a measurement is well described by the uncertainty in that measurement for a given quantity of interest. At least in an averaged sense, the best measurement is the one that produces the lowest uncertainty.

The DOE/SNL Scaled Wind Farm Technology (SWiFT) research wind farm facility contains highly instrumented wind turbines with a suite of atmospheric measurements to produce well characterized, high-resolution validation data.[1] This paper focuses on the uncertainty quantification for blade load measurements using strain gages and the processes required for mapping those measured loads to additional turbine quantities of interest on the SWiFT turbines.

II. Methods

This section describes the methodology required to produce uncertainty estimates from blade mounted strain gage measurements. The methodology is then applied to the quantities of interest of blade-generated aerodynamic torque and thrust. The methodology used to propagate uncertainty in the measurements to the quantity of interest is the standard equation defined by Equation 1. This equation and approach has three general assumptions that the variables, x_i, are uncorrelated with each other, have Gaussian distributions for repeated observations, and that the uncertainty in each variable, δx_i, is representative of the same level (i.e., 95%).

$$\delta X = \sqrt{\sum_{i=1}^{N} \left(\frac{\partial X}{\partial x_i} \delta x_i \right)^2} \tag{1}$$

A. Blade Load Measurement

Blade root loads on the SWiFT turbines are measured using non-metallic fiber optic strain gages with fiber Bragg grating, Micron Optics os3200 sensors. These sensors measure strain directly, which can be used to estimate the bending moment on the portion of the blade outboard of the sensor. However, the transverse shear forces at the measurement location are not directly measured, and their treatment will be described in the next section. The root strain gages are installed on the inside of the blade where it has a circular

cross-section. The inner surface of the blade is not a toleranced dimension and is not perfectly circular, introducing some additional uncertainty. The gages are installed axially by hand, with pairs being nominally 180° offset from each other circumferentially. An additional uncertainty term comes in the form of gage misalignment, θ. Efforts are made to mark and lay the gages axially, but there is an associated level of uncertainty in the installation that is accounted for by this angle. For the OEM V27 blades, there are four sensors positioned every 90° circumferentially along the inner radius. As a result of the purely axial gage position for these sensors, there is no ability for the gage pair to remove the effect of transverse forces or torsional moments which both produce shear strain in the blade that shows up in the strain measured by the sensor. The desire with these pairs of strain gages is to quantify the root bending moments, but what is being measured includes the effect of shear strain. The measurement of a single strain gage subjected to axial strain, ϵ, and shear strain, γ, can be derived geometrically from the understanding of how strain gages measure straing and by approximating the mounting surface as a planar geometry for the gage location, which is accurate for a small gage with low strain levels. By assuming small strain values, the derivation reduces to the standard strain transformation equation[2] described by Equation 2.

$$\epsilon_s = \epsilon\ cos^2\theta - \nu\epsilon\ sin^2\theta + \gamma\ sin\theta cos\theta \tag{2}$$

As described by this equation, the actual strain gage measurement is a result of the multiple component loading on the blade. Since the desired measurement from these gages is the bending moment, and therefore the axial strain only, the shear strain contribution produces an error in the measurement. In order to represent this error through an uncertainty, the axial strain and shear strain must be derived from the loading on the blade. A "global" blade coordinate system is used where Y is in the rotational plane and positive opposite rotation direction, Z is orthogonal to the blade root face and positive towards the blade tip, and X is defined using the cross product $\hat{X} \times \hat{Y} = \hat{Z}$ in a right-handed coordinate system which makes it positive downwind parallel to the tilted rotor shaft.

Axial strain is a result of bending moments (due to spanwise transverse loading along the blade), the axial force due to the centrifugal force and gravity, and the thermal strain caused by a temperature change. Material strain is related to the applied stress through Hooke's law, and the standard calculation of stress from bending moments and from axial forces is used to calculate axial strain as summarized in Equation 3. The determination of strain is dependent upon the gage location (x, y) relative to the neutral axis which is taken as the geometric center of the blade root annulus. The product EI of Young's modulus and the area moment of inertia is calculated by known material properties and dimensions, but this product can also be determined during a calibration of the blade sensors with known loads.

$$\epsilon = \frac{1}{EI}\left[M_X * y - M_Y * x + F_Z\frac{I}{A}\right] + CTE\Delta T \tag{3}$$

Shear strain is produced in the blade section by transverse shear forces and the integrated torsional moment produced along the blade. The shear forces and torsion produce shear stresses that are related to the shear strain by the shear modulus, G, as described in Equation 4. Transverse shear forces that occur a distance away from the cross section of interest are what give rise to the bending moment and axial stress in the cross-section previously discussed. The transverse shear stress is the result of internal resisting forces that arise to balance the variable stress caused by the bending moment in the cross section and sum to balance the shear force, meaning that the shear stress due to transverse loading is zero at the surface furthest from the bending neutral axis and maximum at the neutral axis. The formulation for shear stress arising from a transverse force for a thin wall beam is used. This formulation is appropriate for cross-sections where the thickness is much smaller than its overall dimensions which is true for the airfoil sections of a wind turbine blade and sufficiently accurate for this analysis in the blade root. The shear path for thin wall beams is assumed to be always tangent to the centerline path, $\bar{r}$, of the material thickness and constant through the thickness. The varying shear stress magnitude and direction is determined by the angular displacement in the Z-axis from the shear force orientation, $\theta_{Z,X}$ and $\theta_{Z,Y}$.

$$\gamma = \frac{1}{G}\left[\frac{-F_X * sin\theta_{Z,X}}{\pi\bar{r}t} + \frac{-F_Y * sin\theta_{Z,Y}}{\pi\bar{r}t} + \frac{M_Z * r}{J}\right] \tag{4}$$

Equations 3 and 4 can be used with Equation 2 to solve for the measured sensor strain from a known load set at any point within the circular root. To get an idea of the maximum uncertainty, extreme values of design loads were used as calculated from aeroelastic simulations of the wind turbine for the operational

design load cases described in the governing design standard *IEC 61400-1 Ed.3: Wind turbines - Part 1: Design Requirements*.[3] Using the maximum resultant shear force at the blade root produces a shear strain maximum of 160 micro strain for the SWiFT turbine blade root properties, which produces a maximum uncertainty bound for shear-induced uncertainty in the strain gage measurement. This maximum shear strain would likely differ substantially between the edge and flap directions of the blade, and should be treated separately for estimating final values for the strain uncertainty. As mentioned previously, gage installation misalignment results in the gage measuring axial strain at an angle offset from the pitch axis which introduces additional error, resulting in uncertainty. The uncertainty in the measured axial strain due to the presence of shear strain and gage misalignment is displayed in Figure 1 as a percent error of the actual axial strain, using representative values of blade root axial strain and shear strain.

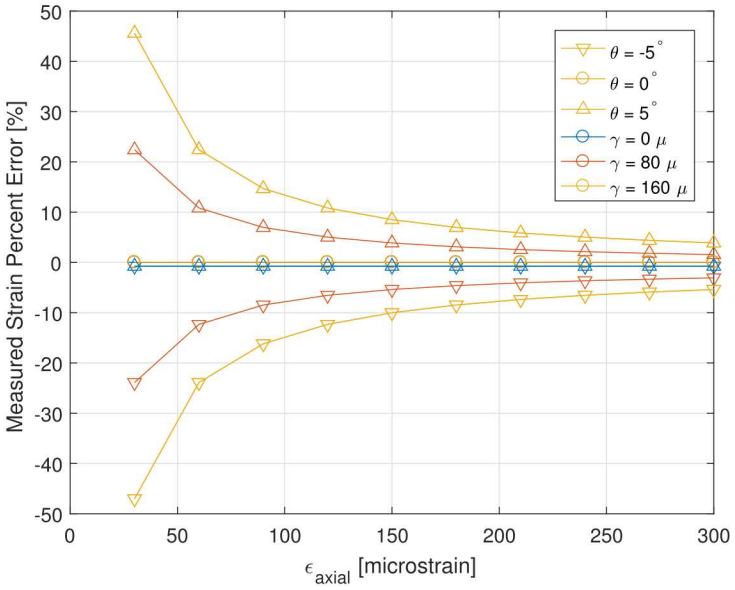

Figure 1. Axial strain measurement uncertainty from shear and gage misalignment angles as a percent error of the mean axial strain (colors represent shear strain levels, markers represent gage misalignment levels).

The figure reveals that the error in axial strain measurement due to shear strain is negligible if the sensor is mounted purely axially, as shown by the lines with circle markers. However, when gage misalignment is present, the additional error caused by shear strain becomes notable and varies with shear strain level, shown by the lines with triangle markers. While the gage misalignment can be present for all values of axial strain, the shear strain levels would vary proportionally to axial strain. The bending moment is a result of the transverse shear forces which produce the shear strain sourced bias, so it is expected that the smaller bending moments will have an accompanying small level of shear strain. This means that the yellow lines are only thought to be accurate at the highest levels of axial strain, and that the errors induced by potential gage misalignment and because of the presence of shear strain likely stay within $\pm 5^\circ$ in the maxima.

This section has considered the uncertainty in the desired measurement of the strain sensor of axial strain due to the reality of this measurement including the effects of shear strain and gage misalignment. The final source of strain measurement uncertainty considered is that of the sensor's measurement of strain itself, $\delta\epsilon_{s,meas}$. These three sources of uncertainty are combined in Equation 5 to produce the total uncertainty in the strain measurement when axial strain is the desired measurand. The uncertainties due to shear strain and gage misalignment are correlated and are treated collectively by the first term.

$$\delta\epsilon_s = \sqrt{\delta\epsilon_{s,\gamma}(\theta)^2 + \delta\epsilon_{s,meas}^2} \tag{5}$$

In order to derive the uncertainty in the measurement of strain, it is important to first describe what is being measured by the sensor. The Micron Optics Hyperion fiber optic interrogator utilizes Fiber Bragg sensor grating to interpret strain as a shift in wavelength produced by the strain gage dimensional elongation. This system has a stated accuracy of ± 1 pm in the measured wavelength, λ_s. Material strain as measured by a strain gage is the combination of mechanical strain and thermal strain. Mechanical strain can further

be decomposed for this application into aerodynamically-induced strain, gravity-induced strain, and a strain bias which arises from installation or other sources. The desired strain component in the measurement is the aerodynamically-induced source, as defined in Equation 9.

$$\epsilon_{total} = \epsilon_{mech} + \epsilon_{thermal} \tag{6}$$

$$\epsilon_{total} = \epsilon_{aero} + \epsilon_{gravity} + \epsilon_{bias} + \epsilon_{thermal} \tag{7}$$

$$\epsilon_{total} = \frac{\Delta\lambda/\lambda_0}{F_G} \tag{8}$$

$$\epsilon_{s,meas} = \epsilon_{aero} = \frac{\Delta\lambda/\lambda_0}{F_G} - \epsilon_{gravity} - \epsilon_{bias} - CTE * \Delta T \tag{9}$$

To obtain the aerodynamically-induced strain measurement, the last three terms in the strain equation must be removed through calibration and calculation. The gravity term can be removed through knowledge of the blade weight, center of mass, and instantaneous position. The mechanical strain bias and coefficient of thermal expansion can be calibrated and removed using long time histories of unloaded blade data undergoing temperature fluctuations. The terms described in Equation 9 each contribute to the uncertainty in the measurement of strain as defined by Equation 10.

$$\delta\epsilon_{s,meas} = \sqrt{\left(\left|\frac{1}{\lambda_0 F_G}\right| \delta\lambda\right)^2 + \delta\epsilon_{gravity}^2 + \delta\epsilon_{bias}^2 + \left(|\Delta T|\, \delta CTE\right)^2 + \left(|CTE|\, \delta T\right)^2} \tag{10}$$

The relationship between strain and bending moment was defined analytically by Equation 3 in order to calculate strain levels from simulated load sets, however, in practice it is typically considered to be more precise to relate the two quantities through calibration. The bending moment is calibrated to the strain differential (as is true for a case with a pure bending moment) which for the SWiFT V27 blade produces a calibration constant of around $K_{cal} = 0.7\ kNm/\mu$. Using the strain differential removes the effect of pure axial strain, such as that due to the centrifugal force. The strain differential also means that a factor of 2 is added to the bending moment uncertainty calculation, Equation 12. The uncertainty in the bending moment depends on the total uncertainty in the strain measurement, as calculated by Equation 5. Using the defined equations, the total uncertainty in the strain measurement and the resulting uncertainty in the bending moment estimate is derived as an example and listed in Table 1. This table also provides insight into the level of contribution to the uncertainty in bending moment from the different sources.

$$M_{bending} = K_{cal}[kNm/\mu] * \Delta\epsilon_s \tag{11}$$

$$\delta M_{bending} = \sqrt{2\left(|K_{cal}|\, \delta\epsilon_s\right)^2 + 2\left(|\epsilon_s|\, \delta K_{cal}\right)^2} \tag{12}$$

B. Blade Load Force Estimation

As described previously, the system of blade strain gages used on the SWiFT turbines do not measure the transverse shear forces on the blade. These resultant forces are needed to map the measured moments to other locations on the turbine when a coordinate translation is performed to map the loads to a quantity of interest that occurs at a separate location. The resultant shear forces at the gage location can be roughly estimated using blade element momentum theory, as shown in Equations 13-14.

$$\frac{dF_\tau}{dr} = \frac{1}{2}\rho U^2 C_l * c * \left((1-a)^2 + TSR^2\left(\frac{r}{R}\right)^2(1+a')^2\right)\left(cos(90^\circ - \phi) - \frac{C_d}{C_l}cos(\phi)\right) \tag{13}$$

$$\frac{dF_T}{dr} = \frac{1}{2}\rho U^2 C_l * c * \left((1-a)^2 + TSR^2\left(\frac{r}{R}\right)^2(1+a')^2\right)\left(sin(90^\circ - \phi) + \frac{C_d}{C_l}sin(\phi)\right) \tag{14}$$

where,

Table 1. Strain measurement and bending moment estimate uncertainty level and source contribution.

Term $[x]$	Units	Uncertainty $[\delta\overline{x}]$
$\delta\epsilon_{total}$	$[\mu]$	0.823
$\delta\epsilon_{gravity}$	$[\mu]$	-
$\delta\epsilon_{bias}$	$[\mu]$	0.823
$\delta\epsilon_{thermal}$	$[\mu]$	1.147
$\delta\epsilon_{s,meas}$	$[\mu]$	1.635
$\delta\epsilon_{s,\gamma}$	$[\%\epsilon]$	2
$\delta\epsilon_s$	$[\mu]$	$\sqrt{(0.02\ \epsilon)^2 + 2.673}$
$\delta M_{bending}$	$[kNm]$	$\sqrt{0.0002\ M_b^2 + 2.62}$

$$\phi = tan^{-1}\left(TSR\frac{r}{R}\left(\frac{1+a'}{1-a}\right)\right) \tag{15}$$

The estimated transverse shear force can be related to the measured moment through a simple linear force loading approximation, as derived in Equations 16-19. This estimation is compared with the blade element momentum theory using some approximations for the SWiFT turbine values in Figure 3 for the torque and thrust directions.

$$F(x) = \frac{-F_0}{l}x + F_0 \tag{16}$$

$$M(x) = \int_x^l \left(\frac{-F_0}{l}x + F_0\right)dx \tag{17}$$

$$M(x) = \frac{F_0}{2l}x^2 - F_0 x + \frac{F_0 l}{2}\ ,\ 0 \leq x \leq l \tag{18}$$

$$\widehat{F_0} = \frac{2M_{0,meas}}{l} \tag{19}$$

The relation in Equation 19 is used in this analysis for estimating the transverse shear forces in a blade from the bending moments, as measured by the blade strain gage sensors. This methodology has relied on rough approximations and will have an associated high uncertainty. In an effort to statistically define this uncertainty under the stochastic operating conditions of a wind turbine, aeroelastic simulations of the SWiFT turbine were performed using turbulent conditions representative of the site. The percent error of the estimated shear resultant force calculated by Equation 19 in comparison with the "true" value from the simulations is shown statistically in Figure 3. The uncertainty in this estimate is calculated for the 95% confidence interval as a percentage of the actual value for the transverse force in the torque (y) direction and the thrust (x) direction, as listed in Equations 20 and 21.

$$\delta\widehat{F}_{x',95\%} = \begin{cases} -52.0\% \\ +31.6\% \end{cases} \tag{20}$$

$$\delta\widehat{F}_{y',95\%} = \begin{cases} -61.2\% \\ +15.5\% \end{cases} \tag{21}$$

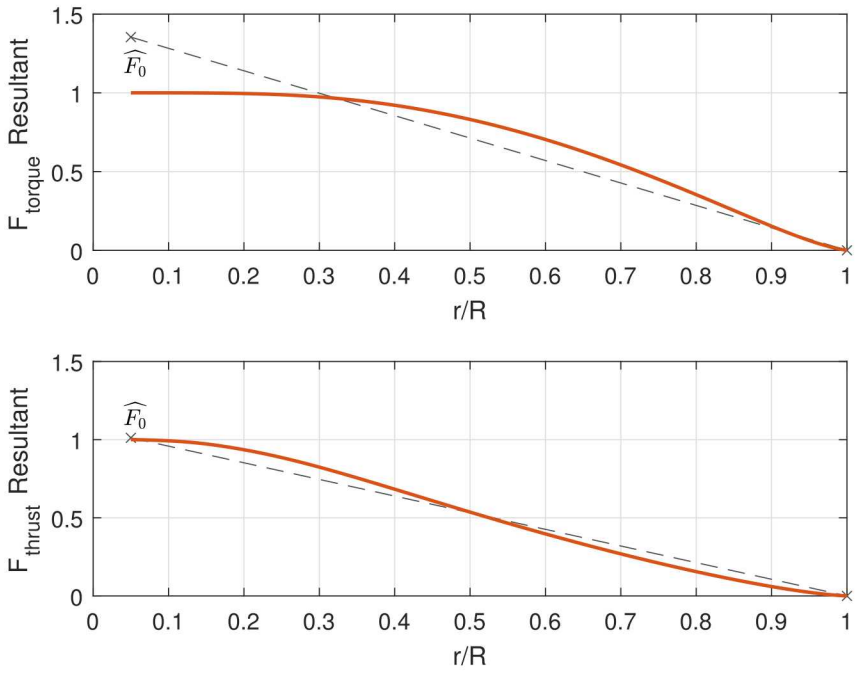

Figure 2. Blade resultant force calculation (red) and estimation (grey).

C. Blade Load Transformation

The measured blade loads can be used to estimate other loads on the system through coordinate transformations of the load set to the desired location and orientation. Equation 22 shows the generic process for coordinate transformation of a load set, which will be derived for coordinate rotation and translation in this section. It is important to note that the translations do not include additional forces and moments that occur between the two coordinate system locations (such as blade root drag inboard of measurement location, tower drag, etc.). Where these forces are thought to be considerable relative to the measured loads or where they produce significant moments when translated over a large distance it will be necessary to estimate the force distributions between the translated coordinate systems.

$$\begin{bmatrix} F_{x2} \\ F_{y2} \\ F_{z2} \\ M_{x2} \\ M_{y2} \\ M_{z2} \end{bmatrix} = \begin{bmatrix} \begin{bmatrix} F/F \\ \\ M/F \end{bmatrix} & \begin{bmatrix} F/M \\ \\ M/M \end{bmatrix} \end{bmatrix} * \begin{bmatrix} F_{x1} \\ F_{y1} \\ F_{z1} \\ M_{x1} \\ M_{y1} \\ M_{z1} \end{bmatrix} \tag{22}$$

The F/F and M/M matrices in Equation 22 are the same as each other, and contain the relation from rotation or translation of the coordinate system. Depending on the operation being performed, these matrices are described by Equations 23-26 below. A translation is seen to not affect the contribution of the resultant force due to translation of a force matrix (F/F), or to affect the contribution of the resultant moment due to the translation of a moment matrix (M/M). However, there will be a contribution of the resultant moment due to the translation of a force, M/F, that depends on the translation magnitude. In the rotation matrices, the rotation angle is referenced from the original coordinate system to the transformed coordinates, using the original coordinate system definition for positive and negative angles.

$$R_x(\theta_x) = \begin{bmatrix} 1 & 0 & 0 \\ 0 & cos\theta_x & sin\theta_x \\ 0 & -sin\theta_x & cos\theta_x \end{bmatrix} \tag{23}$$

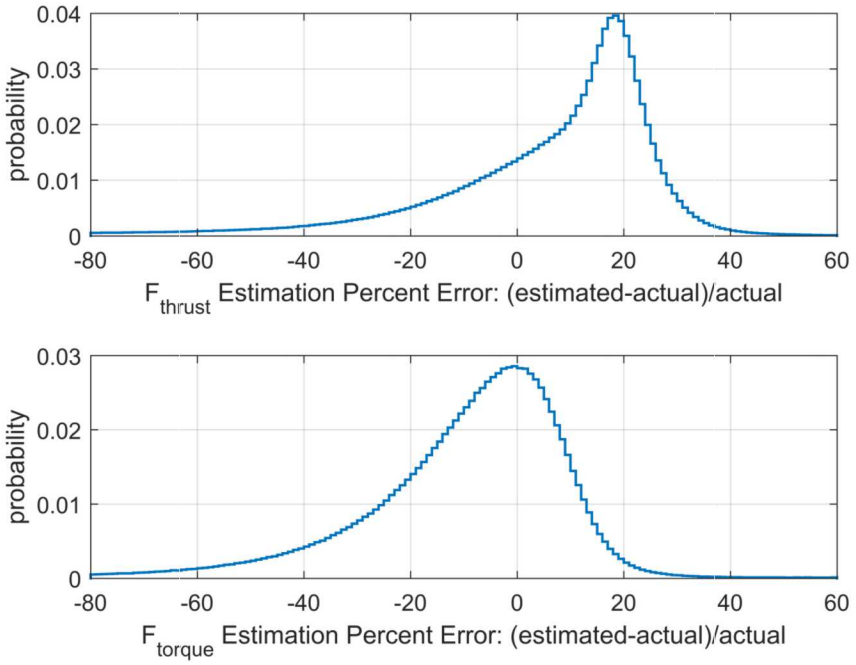

Figure 3. Simulated blade root shear force estimation error.

$$R_y(\theta_y) = \begin{bmatrix} cos\theta_y & 0 & -sin\theta_y \\ 0 & 1 & 0 \\ sin\theta_y & 0 & cos\theta_y \end{bmatrix} \tag{24}$$

$$R_z(\theta_z) = \begin{bmatrix} cos\theta_z & sin\theta_z & 0 \\ -sin\theta_z & cos\theta_z & 0 \\ 0 & 0 & 1 \end{bmatrix} \tag{25}$$

$$T_{xyz} = \begin{bmatrix} 1 & 0 & 0 \\ 0 & 1 & 0 \\ 0 & 0 & 1 \end{bmatrix} \tag{26}$$

The M/F matrix describes the relation of the transformed moment arising from the force matrix in the original coordinate system. For coordinate system translation and rotation, the operation is described in Equation 27 or Equation 28, respectively.

$$(M/F)_T = \begin{bmatrix} 0 & d_z & -d_y \\ -d_z & 0 & d_x \\ d_y & -d_x & 0 \end{bmatrix} \tag{27}$$

$$(M/F)_R = \begin{bmatrix} 0 & 0 & 0 \\ 0 & 0 & 0 \\ 0 & 0 & 0 \end{bmatrix} \tag{28}$$

The F/M matrix describes the contribution to the transformed force from the moment set in the original coordinate system. Regardless of transformation, a moment never contributes to a force and this matrix is therefore a 3x3 zero matrix.

$$F/M = \begin{bmatrix} 0 & 0 & 0 \\ 0 & 0 & 0 \\ 0 & 0 & 0 \end{bmatrix} \tag{29}$$

The matrices defined above are combined into a transformation matrix that can be used for a rotation or a translation of the coordinate system which is described in Equation 30, for the operation defined in Equation 22. While multi-axis translations are commutative, this matrix should only be used for one rotation at a time and then multiplied together to produce the correct transformation matrix.

$$\begin{bmatrix} cos\theta_y cos\theta_z & sin\theta_z & -sin\theta_y & 0 & 0 & 0 \\ -sin\theta_z & cos\theta_x cos\theta_z & sin\theta_x & 0 & 0 & 0 \\ sin\theta_y & -sin\theta_x & cos\theta_x cos\theta_y & 0 & 0 & 0 \\ 0 & d_z & -d_y & cos\theta_y cos\theta_z & sin\theta_z & -sin\theta_y \\ -d_z & 0 & d_x & -sin\theta_z & cos\theta_x cos\theta_z & sin\theta_x \\ d_y & -d_x & 0 & sin\theta_y & -sin\theta_x & cos\theta_x cos\theta_y \end{bmatrix} \tag{30}$$

1. Blade Loads Estimated Aerodynamic Torque

The aerodynamic torque can be estimated from the blade load measurements. The advantage of this measurement is that it is on the rotor side of the drivetrain and generator losses are not added into the uncertainty. However, the measurement is of strain which is used to estimate the bending moment, and force can only be approximated from the measurement as discussed previously. The mapping of the blade loads to aerodynamic torque is done generically for a wind turbine by rotation about the spanwise z-axis to the rotation plane, rotation about the rotation plane axis to account for blade preconing, translation from the measurement plane to the shaft, and finally with rotation about the shaft axis by the blade azimuth. The individual blade forces and moments are then summed when individually mapped onto the non-rotating shaft coordinate system. The transformation from the blade root strain gage measurements to blade loads estimated aerodynamic torque follows the steps listed in Equation 31.

$$R_z(\theta_{rotorplane}) \rightarrow R_z(\beta_0) \rightarrow R_y(\theta_{precone}) \rightarrow T_z(d_{gage}) \tag{31}$$

Performing this set of transformations produces Equation 32 for the aerodynamic torque contribution from each blade.

$$\begin{aligned} \tau_{aero,B} = {} & d_{gage} * sin\beta_0 * (F_{x'} cos\theta_{rotorplane} + F_{y'} sin\theta_{rotorplane}) \\ & - d_{gage} * cos\beta_0 * (-F_{x'} sin\theta_{rotorplane} + F_{y'} cos\theta_{rotorplane}) \\ & + cos\beta_0 * (M_{x'} cos\theta_{rotorplane} + M_{y'} sin\theta_{rotorplane}) \\ & + sin\beta_0 * (-M_{x'} sin\theta_{rotorplane} + M_{y'} cos\theta_{rotorplane}) \end{aligned} \tag{32}$$

$$\tau_{aero,rotor} = \tau_{aero,B1} + \tau_{aero,B2} + \tau_{aero,B3} \tag{33}$$

2. Blade Loads Estimated Rotor Thrust

The blade loads can be transformed to obtain an estimate of the rotor thrust by following a similar procedure as with rotor torque. This approach is unlikely to be as accurate as obtaining the thrust from driveshaft or tower measurements, but it may provide high-frequency content of interest that is unavailable from other measurement sources. The load transformation follows the rotations and translations outlined in Equation 34, with the result for blade loads estimated thrust given by Equation 35.

$$R_z(\theta_{rotorplane}) \rightarrow R_z(\beta_0) \rightarrow R_y(\theta_{precone}) \rightarrow T_z(d_{gage}) \rightarrow R_x(-\psi) \rightarrow R_y(-\theta_{shafttilt}) \tag{34}$$

$$
\begin{aligned}
T_B = & cos\theta_{shafttilt} * cos\beta_0 * (F_{x'} cos\theta_{rotorplane} + F_{y'} sin\theta_{rotorplane}) \\
& + cos\theta_{shafttilt} * sin\beta_0 * (-F_{x'} sin\theta_{rotorplane} + F_{y'} cos\theta_{rotorplane}) \\
& - sin\theta_{shafttilt} * sin\psi * sin\beta_0 * (F_{x'} cos\theta_{rotorplane} + F_{y'} sin\theta_{rotorplane}) \\
& + sin\theta_{shafttilt} * sin\psi * cos\beta_0 * (-F_{x'} sin\theta_{rotorplane} + F_{y'} cos\theta_{rotorplane}) \\
& + sin\theta_{shafttilt} * cos\psi * F_{z'}
\end{aligned} \tag{35}
$$

$$
T_{rotor} = T_{B1} + T_{B2} + T_{B3} \tag{36}
$$

III. Results

Propagation of uncertainty of the blade load measurement. force estimation, and transformation produces the uncertainty estimate for blade load estimated torque and thrust. Starting with the equations for torque and thrust the uncertainty is a sum of squares of the partial derivatives of the quantity with the variable, multiplied with the uncertainty in the individual measurement variables. Equations 37 and 38 show the full list of measurement variables that produce the total uncertainty in blade measured torque and thrust, for a single blade. The total rotor uncertainty could be obtained by treating the blades as having equivalent uncertainties, and would be the product of the blade uncertainty and $\sqrt{3}$, i.e., $\delta\tau_{rotor} = \sqrt{3}\delta\tau_B$. The intent of this paper is not to produce an actual estimate of the uncertainty for blade measured loads, but rather to define the methodology and show qualitative sensitivities to the input variables. For this reason, the comparison will be made using the blade uncertainty, as opposed to the rotor uncertainty.

$$
\begin{aligned}
\delta\tau^2_{aero,B} = & \left(\left|\frac{\partial\tau_B}{\partial M_{x'}}\right|\delta M_{x'}\right)^2 + \left(\left|\frac{\partial\tau_B}{\partial M_{y'}}\right|\delta M_{y'}\right)^2 + \left(\left|\frac{\partial\tau_B}{\partial F_{x'}}\right|\delta F_{x'}\right)^2 + \left(\left|\frac{\partial\tau_B}{\partial F_{y'}}\right|\delta F_{y'}\right)^2 + \\
& \left(\left|\frac{\partial\tau_B}{\partial d_{gage}}\right|\delta d_{gage}\right)^2 + \left(\left|\frac{\partial\tau_B}{\partial\beta_0}\right|\delta\beta_0\right)^2 + \left(\left|\frac{\partial\tau_B}{\partial\theta_{rotorplane}}\right|\delta\theta_{rotorplane}\right)^2
\end{aligned} \tag{37}
$$

$$
\begin{aligned}
\delta T^2_B = & \left(\left|\frac{\partial T_B}{\partial F_{x'}}\right|\delta F_{x'}\right)^2 + \left(\left|\frac{\partial T_B}{\partial F_{y'}}\right|\delta F_{y'}\right)^2 + \left(\left|\frac{\partial T_B}{\partial F_{z'}}\right|\delta F_{z'}\right)^2 + \left(\left|\frac{\partial T_B}{\partial\theta_{shafttilt}}\right|\delta\theta_{shafttilt}\right)^2 \\
& + \left(\left|\frac{\partial T_B}{\partial\theta_{rotorplane}}\right|\delta\theta_{rotorplane}\right)^2 + \left(\left|\frac{\partial T_B}{\partial\beta_0}\right|\delta\beta_0\right)^2 + \left(\left|\frac{\partial T_B}{\partial\psi}\right|\delta\psi\right)^2
\end{aligned} \tag{38}
$$

The full expansion of the torque and thrust uncertainty equations will not be shown in this paper, but the inputs required for quantifying the torque and thrust uncertainties are approximated for three wind speed conditions and listed in Tables 2-4. Representative values for the two bending moments as would be measured by the strain gage pairs are obtained from a set of aeroelastic wind turbine simulations in turbulent flow conditions in order to represent likely loading conditions. These three sets on input variables are used with Equations 37 and 38 to quantify the $1 * \sigma$ uncertainty for a single blade in torque and thrust estimates. Results from these calculations are shown in Figures 4 and 5 for the three different operating conditions.

Figures 4 reveal that by far the largest contributor to uncertainty in the torque estimate from blade measurements is the uncertainty caused by $\delta M_{x'}$. This edgewise moment is the largest contributor to the torque estimate, and also has a substantial level of uncertainty relative to its mean. This uncertainty source was defined by Equation 12 and produces a high level of uncertainty due to the stated accuracy of the fiber optic interrogator system and the low levels of strain in the measurement root region of the blade. A surprising feature of this analysis is that the second highest contributor to uncertainty in torque is the uncertainty in the rotational location of the strain gage sensor pair, $\theta_{rotorplane}$. In order to reduce the uncertainty in the torque estimate, it should be attempted to reduce uncertainty in the strain measurement and calibration uncertainty.

Figures 5 reveal the largest contributors to uncertainty in the blade approximated thrust force. One particularly surprising result is that although the thrust force depends entirely on the blade root forces which aren't measured directly by the strain gages, the resulting uncertainty is actually lower than the uncertainty in the torque measurement in some conditions. Looking at the contributors to uncertainty in thrust it is apparent that the uncertainty in the resultant force nominally in the downwind direction, $F_{x'}$, has the most influence on uncertainty levels in the thrust estimate. The implication of this finding is that

Table 2. Representative mean values and variable uncertainty at site mean wind speed conditions (7 m/s).

Variable [x]	Units	Mean $[\overline{x}]$	Uncertainty $[\delta\overline{x}]$
$M_{x'}$	[kNm]	4.0	1.62
$M_{y'}$	[kNm]	34.4	1.69
$F_{x'}$	[kN]	$2M_{y'}/l = 5.3$	(-1.38, +0.84)
$F_{y'}$	[kN]	$-2M_{x'}/l = -0.6$	(-0.19, +0.05)
$F_{z'}$	[kN]	$m_B r_{CG}\Omega^2 = 50.2$	1.29
d_{gage}	[m]	0.75	0.005
β_0	[deg]	0	0.1
$\theta_{rotorplane}$	[deg]	1	0.5
$\theta_{shafttilt}$	[deg]	4	0.04
ψ	[deg]	0:360	0.04

Table 3. Representative mean values and variable uncertainty at the SWiFT turbine rated wind speed condition (11 m/s).

Variable [x]	Units	Mean $[\overline{x}]$	Uncertainty $[\delta\overline{x}]$
$M_{x'}$	[kNm]	10.8	1.63
$M_{y'}$	[kNm]	55.8	1.80
$F_{x'}$	[kN]	$2M_{y'}/l = 8.6$	(-2.23, +1.36)
$F_{y'}$	[kN]	$-2M_{x'}/l = -1.7$	(-0.51, +0.13)
$F_{z'}$	[kN]	$m_B r_{CG}\Omega^2 = 65.2$	1.67
d_{gage}	[m]	0.75	0.005
β_0	[deg]	0	0.1
$\theta_{rotorplane}$	[deg]	1	0.5
$\theta_{shafttilt}$	[deg]	4	0.04
ψ	[deg]	0:360	0.04

Table 4. Representative mean values and variable uncertainty at SWiFT turbine Region 3 operation (15 m/s).

Variable [x]	Units	Mean $[\overline{x}]$	Uncertainty $[\delta\overline{x}]$
$M_{x'}$	[kNm]	5.5	1.62
$M_{y'}$	[kNm]	39.2	1.71
$F_{x'}$	[kN]	$2M_{y'}/l = 6.0$	(-1.57, +0.95)
$F_{y'}$	[kN]	$-2M_{x'}/l = -0.8$	(-0.26, +0.07)
$F_{z'}$	[kN]	$m_B r_{CG}\Omega^2 = 65.6$	1.68
d_{gage}	[m]	0.75	0.005
β_0	[deg]	11	0.1
$\theta_{rotorplane}$	[deg]	1	0.5
$\theta_{shafttilt}$	[deg]	4	0.04
ψ	[deg]	0:360	0.04

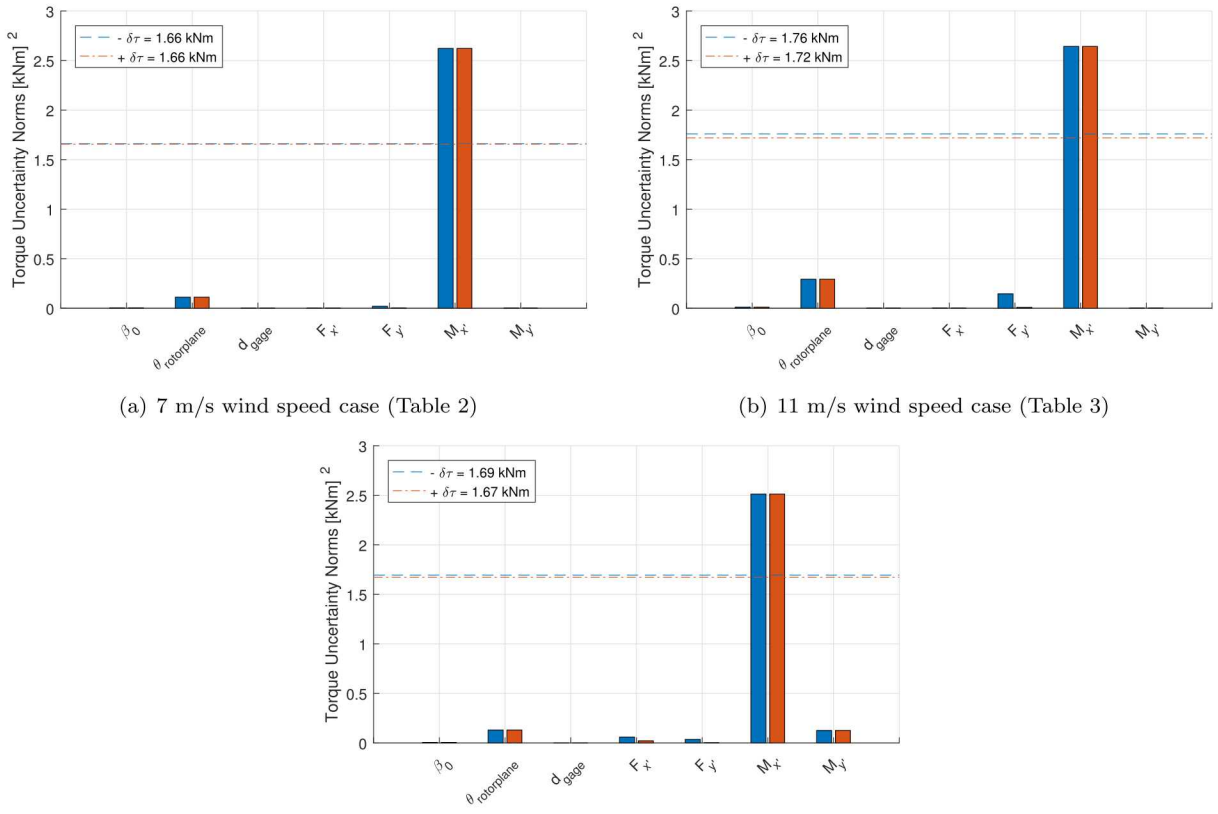

(a) 7 m/s wind speed case (Table 2)

(b) 11 m/s wind speed case (Table 3)

(c) 15 m/s wind speed case (Table 4)

Figure 4. Blade load estimated torque uncertainty quantification with constituent variable norms for negative and positive $1 * \sigma$ uncertainty.

it would not be worth the effort to try to reduce uncertainty in any other quantity if the objective was to minimize uncertainty in the thrust estimate.

IV. Conclusion

A methodology was developed to quantify the uncertainty in rotor torque from blade-measured strain gages, and was extended to include uncertainty in thrust estimates. This methodology was applied to example cases using the SWiFT V27 rotors, revealing the sensitivities to the different measurements and variables in the estimation of these rotor quantities of interest. From this analysis, the uncertainty in torque estimates is driven mostly by uncertainty in the bending moment estimates from strain measurements. The second highest contributor to the uncertainty in torque was due to the uncertainty in strain gage angular location within the blade root, which was a surprising finding. The importance of controlled strain gage temperature compensation and accurate calibration of strain to moment is seen in the significant values for bending moment uncertainty, and its contribution to uncertainty in the estimated torque. The thrust estimate comes completely from blade force estimates, which are not directly measured by strain gages. It is interesting to note that these uncertainties, although dependent on rough approximations for the blade transverse shear forces from strain measurements, appear to at times have relatively comparable values when compared to the torque uncertainty estimates. The values for the uncertainties calculated in this paper should not be treated as quantitative data to be used at this stage, but as an exercise of the methodology developed and defined which will later be combined with precise estimates for the input uncertainties through ongoing work.

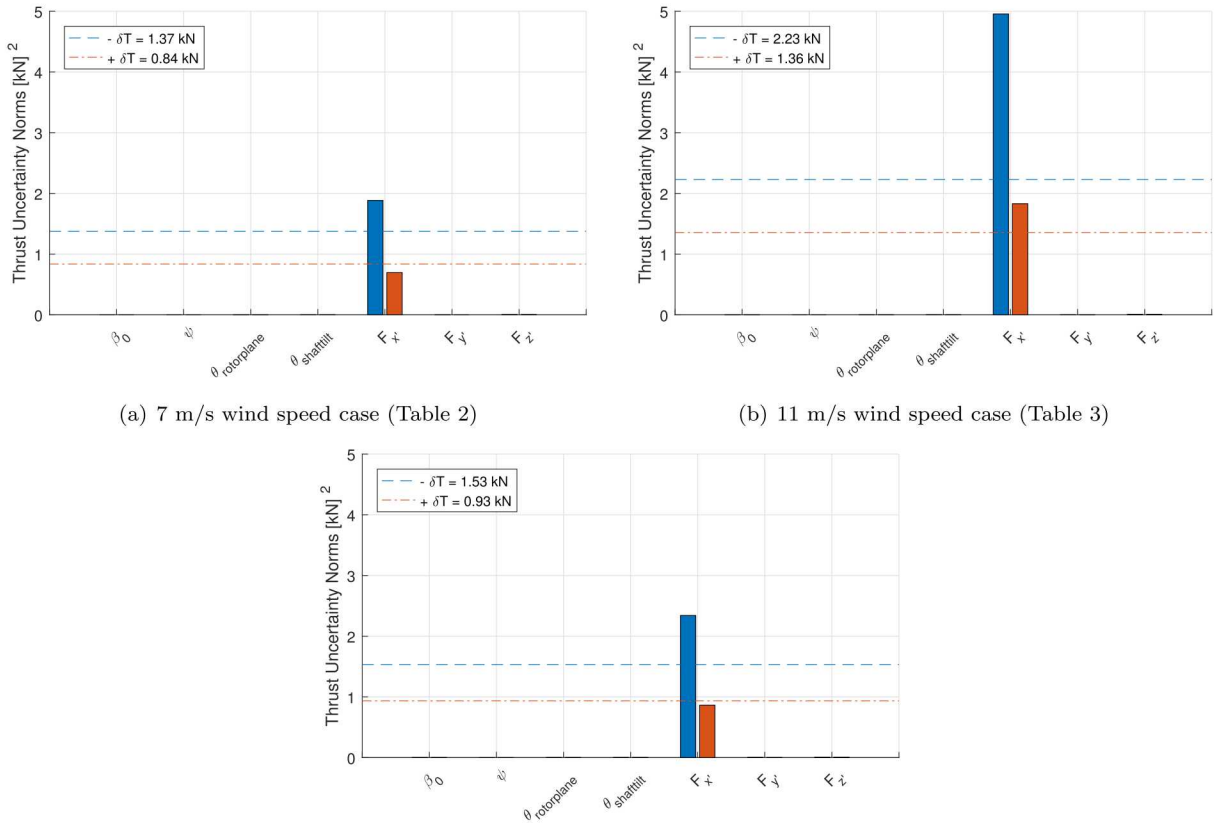

(a) 7 m/s wind speed case (Table 2)

(b) 11 m/s wind speed case (Table 3)

(c) 15 m/s wind speed case (Table 4)

Figure 5. Blade load estimated thrust uncertainty quantification with constituent variable norms for negative and positive $1 * \sigma$ uncertainty.

Acknowledgments

This work was funded by the Wind Energy Technologies Office within the Department of Energy. The experimental uncertainty quantification work at Sandia is being performed as part of the high-fidelity modeling verification and validation efforts within the Atmosphere to Electrons (A2e) program.

References

[1]Berg, J., Bryant, J., LeBlanc, B., Maniaci, D. C., Naughton, B., Paquette, J. A., Resor, B. R., White, J. and Kroeker, D., "Scaled Wind Farm Technology Facility Overview," *32nd ASME Wind Energy Symposium*, American Institute of Aeronautics and Astronautics, 2014.

[2]Dally, J. W. and Riley W. F., *Experimental Stress Analysis*, 1991.

[3]*IEC 61400-1 Ed.3: Wind turbines - Part 1: Design Requirements*, 2005.